Materials Research Express

Nanomechanical behavior of $Pb(Fe_{0.5-x}Sc_xNb_{0.5})O_3$ multiferroic ceramics

To cite this article before publication: Davinder Singh *et al* 2018 *Mater. Res. Express* in press https://doi.org/10.1088/2053-1591/aade3b

Nanomechanical behavior of $Pb(Fe_{0.5-x}Sc_xNb_{0.5})O_3$ multiferroic ceramics

Davinder Singh[1], B Mallesham[2], Akshay Deshinge[1], Kunal Joshi[1], R Ranjith[2], Viswanath Balakrishnan*[1]

[1]*School of Engineering, Indian Institute of Technology Mandi, Kamand, 175005, Himachal Pradesh, India.*

[2]*Department of Materials Science and Metallurgical Engineering, Indian Institute of Technology Hyderabad, kandi, Sangareddy - 502285, Telangana, India*

**viswa@iitmandi.ac.in*

Nanomechanical behavior of $Pb(Fe_{0.5-x}Sc_xNb_{0.5})O_3$ multiferroic ceramics

Abstract:

Nanomechanical behavior of $Pb(Fe_{0.5-x}Sc_xNb_{0.5})O_3$ [(PFSN) ($0 \leq x \leq 0.4$)] was investigated with systematic variation in Sc content to capture the effect of doping induced structural phase transition on mechanical properties. Reduced modulus initially decreased with increase in doping concentration up to 0.2% of Sc content and then showed increment with further addition of Sc. In situ nanoindentation has been carried out from room temperature to 140 °C to measure the variation in reduced modulus and hardness values with temperature in $Pb(Fe_{0.5}Nb_{0.5})O_3$ without Sc addition. Hardness and reduced modulus values of $Pb(Fe_{0.5}Nb_{0.5})O_3$ were found increase from 60 to 100 °C indicating the role of phase transition.

1. Introduction

Perovskite materials showing coexistence of both magnetic and electric ordering have gained extensive attention worldwide due to their complementary properties [1,2]. In particular many perovskites, classified as multiferroics materials, have applications in sensors, actuators and memory and electromechanical devices [3–6]. The coupling phenomenon, especially between magnetic and electric ordering, makes these multiferroics suitable for broad range of applications. The flexibility in perovskite structure allows the synthesis of a wide range of interesting and useful materials. Multiferroic relaxors exhibit complex perovskite structure [General formula: $A(B'B'')O_3$, B'- low valence cation (Fe 3p), and B" high valence cation (Nb 5p , Ta 5p , W 6p)]. One of the widely studied multiferroic pervoskite material is lead iron niobate $Pb(Fe_{0.5}Nb_{0.5})O_3$ (PFN) that shows antiferromagnetic, ferroelectric and structural transitions[7,8]. PFN belongs to a special class of multiferroic relaxors whose properties are found to be modified by cationic substitution [8,9]. It is also considered to be a potential candidate for understanding the basic science involved in the magneto-electric coupling in multi-ferroic relaxors [10]. PFN exhibits electrical and magnetic orders simultaneously that makes it a potential candidate for various magnetic sensors and piezoelectric transducers applications [11–13]. The device realization from piezoelectric ceramics is difficult as they are susceptible to cracking at all scales ranging from electrical domains to devices. Hence investigation of mechanical behavior is important and can provide major insights into failure mechanism of piezoelectric ceramics especially with foreign ion substitution and temperature variation. In addition, the role of phase transition and/or direct application of external pressure on the mechanical behavior are important for developing piezoelectric ceramics based devices. Recently, temperature and doping induced structural transitions have been reported in PFN

ceramics by detailed structural investigations[11,12]. However, the thermomechanical response of PFN to applied loading has not been explored so far. Nanohardness and reduced modulus of Sc doped PFN (PFSN) is measured using nanoindentation. We investigated how systematic variation in Sc doping influences the nanomechanical behavior. In addition, we also performed in situ nanoindentation tests on polycrystalline samples of PFN at various temperatures between 30 °C to 140 °C to capture the role of thermally driven phase transition on nanomechanical properties. The outcome of this work leads to, understanding the mechanical behavior of PFN and PFSN for nano-electromechanical devices and applications design, and will add to the general body of knowledge of the mechanical properties of oxide perovskites.

2. Experimental Procedure

$Pb(Fe_{(0.5-x)}Sc_xNb_{0.5})O_3$ [x = 0, 0.15, 0.2, , 0.3, 0.4] powders were synthesized through solid state reaction route using Wolframite precursor method. Wolframite precursor method is a two-step solid state reaction route, in which initially appropriate precursor is synthesized and PbO added to precursor to achieve the desired compound. For this purpose, initially appropriate Wolframite precursors such as $FeNbO_4$, $ScNbO_4$ are prepared using high pure precursor oxides Fe_2O_3, Nb_2O_5 and Sc_2O_3 (99.9%, make: Sigma Aldrich). To obtain the phase pure Wolframite precursor respective oxides are stoichiometrically taken, homogeneously mixed in an agate mortar using acetone as wetting media. These homogeneous oxide mixtures are calcined at three different temperatures 1000 °C, 1100 °C and 1200 °C for 6 hrs with intermediate grinding to obtain single phase precursors. The obtained phase pure precursors and lead oxide (PbO) were homogeneously mixed using acetone as wetting media to synthesize $Pb(Fe_{0.5-x}Sc_xNb_{0.5})O_3$ compounds. Excess lead oxide (PbO) of 3 wt% is added to maintain the stoichiometry due to volatilization of PbO

during sintering. Homogeneously mixed powders were calcined at two different temperatures 800 °C, 850 °C for 4 hrs to get the single phase compounds with intermediate grinding. Calcined phase powders were ball milled for 6 hrs using agate balls and vials to obtain ultrafine particles. Thus, obtained ultrafine powders were utilized for sintering to achieve high dense pellets.

Homogeneously mixed ultra-fine powders were used to prepare circular pellets of 6 mm diameter. Green pellets were prepared using uniaxial hydraulic press with 6 mm die by applying 2 Ton load. Prior to prepare green pellets, binder polyvinyl alcohol (PVA) added to increase the adhesion between particles. Green pellets were sintered at 1050 °C in muffle furnace by keeping them in a closed alumina crucible. Structural analysis of calcined and sintered powders carried out using X-ray diffractometer [Make: PANalytical: Model: X-pert Pro]. Surface morphology and elemental analysis was done with FEI Nova NANO SEM interfaced with energy dispersive x ray spectroscopy (EDS). In situ nanoindentation tests were performed using Hysitron Triboindentor TI 950.

3. Results and Discussion

Figure 1a shows x-ray diffraction patterns of sintered powders at 1050 °C for 4 hrs. Diffraction patterns clearly reveal that apart from reflections of perovskite phase, a small Bragg reflection (222) around 29.15° is observed corresponding to pyrochlore phase [$Pb_3Nb_4O_{13}$]. However, pyrochlore is present in only with compositions with x = 0.1 0.15, 0.2, 0.25. The volume fraction of pyrochlore phase in these compositions is ≤ 2% calculated using a well-known relation[12].

$$Vol.Fraction\ of\ pyrocholre(\%) = \frac{I_{pyro(222)}}{I_{pyro(222)} + I_{pero(110)}} \times 100\% \quad \ldots (1)$$

With increasing at% of Sc, position of all reflections shifts towards lower Bragg angle due to high ionic radius of Sc^{3+} (74 pm) compare to Fe^{3+} (55 pm). Inset shows an enlarged profile of pseudo cubic (200) reflection, and it shows the gradual peak shift to lower Bragg angles with increasing Sc content from x = 0 - 0.4. Scandium substitution leads to an expansion of unit cell volume due to larger ionic radius of Sc^{3+} (74.5 pm) compared to Fe^{3+} (64.5 pm and 55 pm in high spin and low spin state respectively). The changes in unit cell dimensions are evidenced from the shift of various peak positions towards lower Bragg angle with increasing scandium content. Moreover, our structural analysis in earlier report reveals that structure transforms from monoclinic (space group – Cm) to Rhombohedral (space group – R3m) crystal symmetry [12].

Surface morphology of PFN samples were studied using FESEM and the all samples with and without doping showed similar surface morphology. Figure 1b shows morphology of PFN00 sample having very smooth surface suitable for further nanoindentation studies. Nanoindentation tests were performed on pure PFN and Scandium substituted PFN (PFSN) samples at room temperature. Figure 2a shows a comparison between typical nanoindentation curves obtained from different samples. These applied load versus penetration depth plots were obtained by thrusting the diamond indenter into the surface of sample at a loading rate of 200 μN/s, holding at peak load for 2 seconds and unloading at similar rate. Here we observe that for the same applied load, as we increase the Sc content from x = 0 to 0.2 (code named PFN00 to PFN02) the penetration depth is increasing. However, for samples having Sc content of x = 0.3, 0.4 (code named PFN03 to PFN04) the penetration depth is very low. This suggests that the samples having higher Sc content are more resistant to deformation caused by externally applied load. Inset shows a typical indent impression taken using in situ SPM imaging capability of nanoindenter. Further multiple indents at various applied maximum loads were performed and

nanohardness, H and reduced (or combined) modulus, Er was calculated using Oliver and Pharr method[14]. The standard area function required to calculate these properties was obtained empirically by making several indents on standard fused quartz sample. Figure 2b compares the nanohardness of pure PFN with doped samples. Here nanohardness is within the error limits for all samples and found to be increasing above (x = 0.25) Sc content. This shows that rhombohedral PFN04 has more resistance to plastic deformation. Overall mechanical strength of PFN increases as it undergoes phase transition from monoclinic to rhombohedral, as evident from Figure 2c. Reduced modulus, Er indicates combined modulus of material and diamond nanoindentor is well defined in contact mechanics [15,16]. In Figure 2c Er decreases as Sc content is increased from x = 0 to 0.2. This is due to the expansion in unit cell structure of pure PFN as ionic radii of Sc is more than Fe [17]. Further addition of Sc completely distorts monoclinic unit cell, structural phase transition occurs from monoclinic to rhombohedral and we observe that rhombohedral phase of PFN has increased modulus as compared to monoclinic phase.

Further, we studied the mechanical behavior of pure PFN with respect to increase in temperature. This kind of multiferrioc relaxor undergoes diffused dielectric phase transition with increase in temperature [18]. During this diffused transition, volume of the multiferroic ceramics was found to decrease with increase in temperature. Figure 3a shows different applied load vs penetration depth curves at different temperatures. As expected, plastic deformation is increasing with increase in temperature, however at temperature above 60°C and below 120 °C we observe non monotonous trend in nanohardeness and reduced modulus. This trend is different than the trend observed for similar class of piezoelectric ceramics like PZT [19]. Figure 3b shows variation of nanohardness of pure PFN with respect to temperature. Typically, hardness decreases with

increase in temperature and the observed decreasing trend is consistent with the expectation up to 60°C. Nevertheless, nanohardness of pure PFN starts to increase above 60ºC, which may be due to diffused phase transition. Also, similar trend is observed during temperature dependent Raman study of pure PFN indicating a correlation between hardness and B-localized rotational modes. B-localized mode, which is related to structural distortion softens with temperature upto 100 °C explaining the observed hardness trend[11]. Variation of reduced modulus with increase in temperature is plotted in Figure 3c and we observed a jump in modulus values at around 120°C. Interestingly, two ferroelectric phase transitions in single crystal PFN has also been shown around 100 °C [20] and further studies are needed to achieve direct correlation between the observed mechanical behavior trend with respect to thermally driven phase transition.

4. Conclusions

Solid state synthesis technique was employed to make high purity PFN multiferroic ceramics with varying degree of doping content of Sc. Phase transition in PFN was confirmed with X ray diffraction and Raman studies. Effect of Sc doping was found to increase the reduced modulus and hardness of the pure PFN due to involved structural phase transition from monoclinic to rhombohedral. Furthermore, the effect of temperature on mechanical behavior of pure PFN across the reported phase transition is also confirmed the abrupt variation in nanomechanical properties.

Acknowledgements

We acknowledge Advanced Materials Research Centre at IIT Mandi for characterization facilities and Department of Science and Technology (DST) for funding. One of the authors R Ranjith would like to acknowledge DST-India Fast Track scheme (Project No: SR/FTP/PS-170/2012) for the funding of the project. Davinder Singh and B Mallesham would like to thank Ministry of Human Resource Development (MHRD), Government of India for providing fellowship.

Keywords: phase transition; nanoindentation; multiferroic; hardness; mechanical properties

References:

[1] Ahn K H, Lookman T and Bishop A R 2004 Strain-induced metal–insulator phase coexistence in perovskite manganites *Nature* **428** 401–4

[2] Noheda B, Cox D E, Shirane G, Guo R, Jones B and Cross L E 2001 Stability of the monoclinic phase in the ferroelectric perovskite $PbZr_{1-x}Ti_xO_3$ *Phys. Rev. B - Condens. Matter Mater. Phys.* **63** 014103

[3] Wu S M, Cybart S A, Yu P, Rossell M D, Zhang J X, Ramesh R and Dynes R C 2010 Reversible electric control of exchange bias in a multiferroic field-effect device *Nat. Mater.* **9** 756–61

[4] Vopson M M 2015 Fundamentals of multiferroic materials and their possible applications *Crit. Rev. Solid State Mater. Sci.* **40** 223–50

[5] Surowiak Z and Bochenek D 2008 Multiferroic materials for sensors, transducers and memory devices *Arch. Acoust.* **33** 243–60

[6] Sreenivasulu G, Laletin U, Petrov V M, Petrov V V. and Srinivasan G 2012 A permendur-piezoelectric multiferroic composite for low-noise ultrasensitive magnetic field sensors *Appl. Phys. Lett.* **100** 173506

[7] Wang J T, Mbonye M K and Zhang C 2003 Dielectric, piezoelectric and magnetic properties of ferroelectromagnet $Pb(Fe_{(1/3)}Nb_{(2/3)})O_3$ (PFN) ceramics *Int. J. Mod. Phys. B* **17** 3732–7

[8] Wójcik K, Zieleniec K and Milata M 2003 Electrical Properties of Lead Iron Niobate PFN *Ferroelectrics* **289** 107–20

[9] A-M Welsch, B Mihailova, M Gospodinov, R Stosch B G and U B 2009 High pressure Raman spectroscopic study on the relaxor ferroelectric $PbSc_{0.5}Nb_{0.5}O_3$ *J. Phys. Condens. Matter* **21** 235901

[10] Lente M H, Guerra J D S, De Souza G K S, Fraygola B M, Raigoza C F V, Garcia D and Eiras J A 2008 Nature of the magnetoelectric coupling in multiferroic $Pb(Fe_{1/2}Nb_{1/2})O_3$ ceramics *Phys. Rev. B - Condens. Matter Mater. Phys.* **78** 054109

[11] Mallesham B, Viswanath B and Ranjith R 2016 Effect of crystal structure and cationic order on phonon modes across ferroelectric phase transformation in $Pb(Fe_{0.5-x}Sc_xNb_{0.5})O_3$ bulk ceramics *AIP Adv.* **6** 015116

[12] Mallesham B, Ranjith R and Manivelraja M 2014 Scandium induced structural transformation and B':B' cationic ordering in $Pb(Fe_{0.5}Nb_{0.5})O_3$ multiferroic ceramics *J. Appl. Phys.* **116** 034104

[13] García-Flores A F, Tenne D A, Choi Y J, Ren W J, Xi X X and Cheong S W 2011 Temperature-dependent Raman scattering of multiferroic $Pb(Fe_{(1/2)}Nb_{(1/2)})O_3$. *J. Phys. Condens. Matter* **23** 015401

[14] Oliver C and Pharr M 1992 An improved technique for determining hardness and elastic modulus using load and displacement sensing indentation experiments *J. Mater. Res.* **7** 1564–83

[15] Pharr G M, Oliver W C and Brotzen F R 1992 On the generality of the relationship among contact stiffness, contact area, and elastic modulus during indentation *J. Mater. Res.* **7** 613–7

[16] Arjun Dey A K M 2014 *Nanoindentation of Brittle Solids* (CRC Press)

[17] Wachtel E and Lubomirsky I 2011 The elastic modulus of pure and doped ceria *Scr. Mater.* **65** 112–7

[18] Tsurumi T, Soejima K, Kamiya T and Daimon M 1994 Mechanism of diffuse phase transition in relaxor ferroelectrics *Jpn. J. Appl. Phys.* **33** 1959–64

[19] Li Y, Feng S, Wu W and Li F 2015 Temperature dependent mechanical property of PZT film: An investigation by nanoindentation *PLoS One* **10** 1–15

[20] Kania A, Talik E and Kruczek M 2009 X-Ray Photoelectron Spectroscopy, Magnetic and Dielectric Studies of $PbFe_{1/2}Nb_{1/2}O_3$ Single Crystals *Ferroelectrics* **391** 114–21

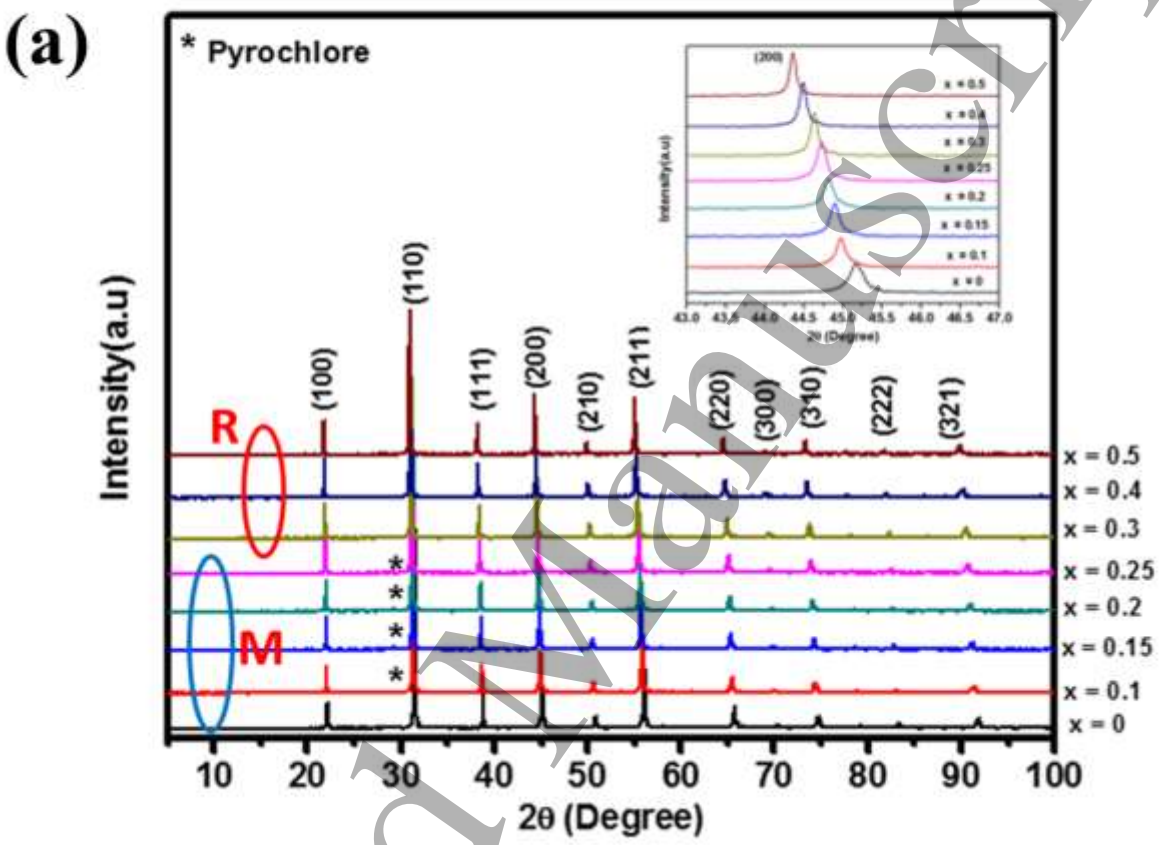

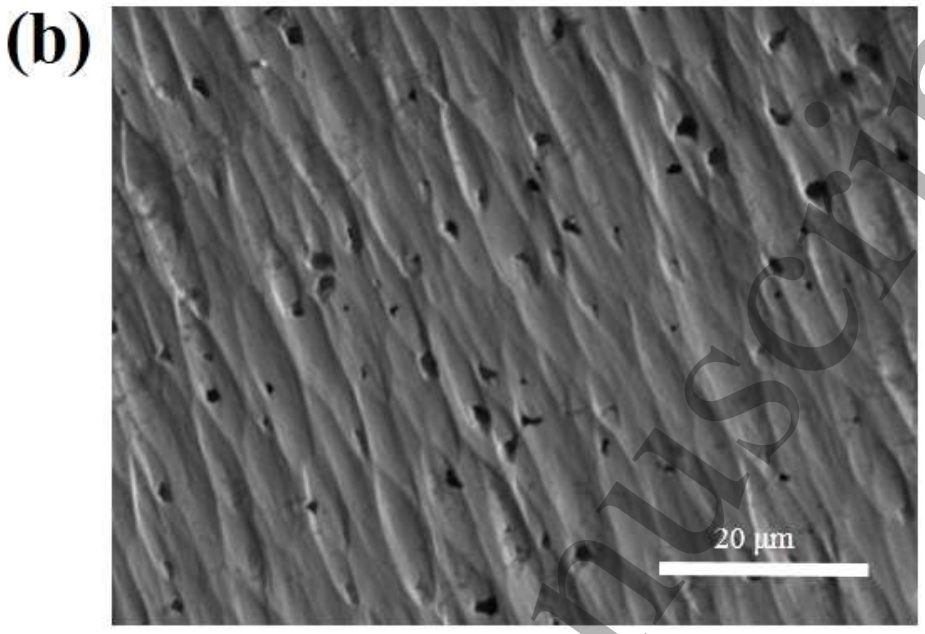

Figure 1 a) X-ray diffraction patterns of Pb $(Fe_{0.5-x}Sc_xNb_{0.5})O_3$ $[0 \leq x \leq 0.5]$ sintered at 1050 °C for 4hrs [In figure pattern covered by blue oval stabilized in monoclinic symmetry, patterns covered by red oval stabilized in rhombohedral symmetry]. b) FESEM image of PFN00 sample with elongated grains.

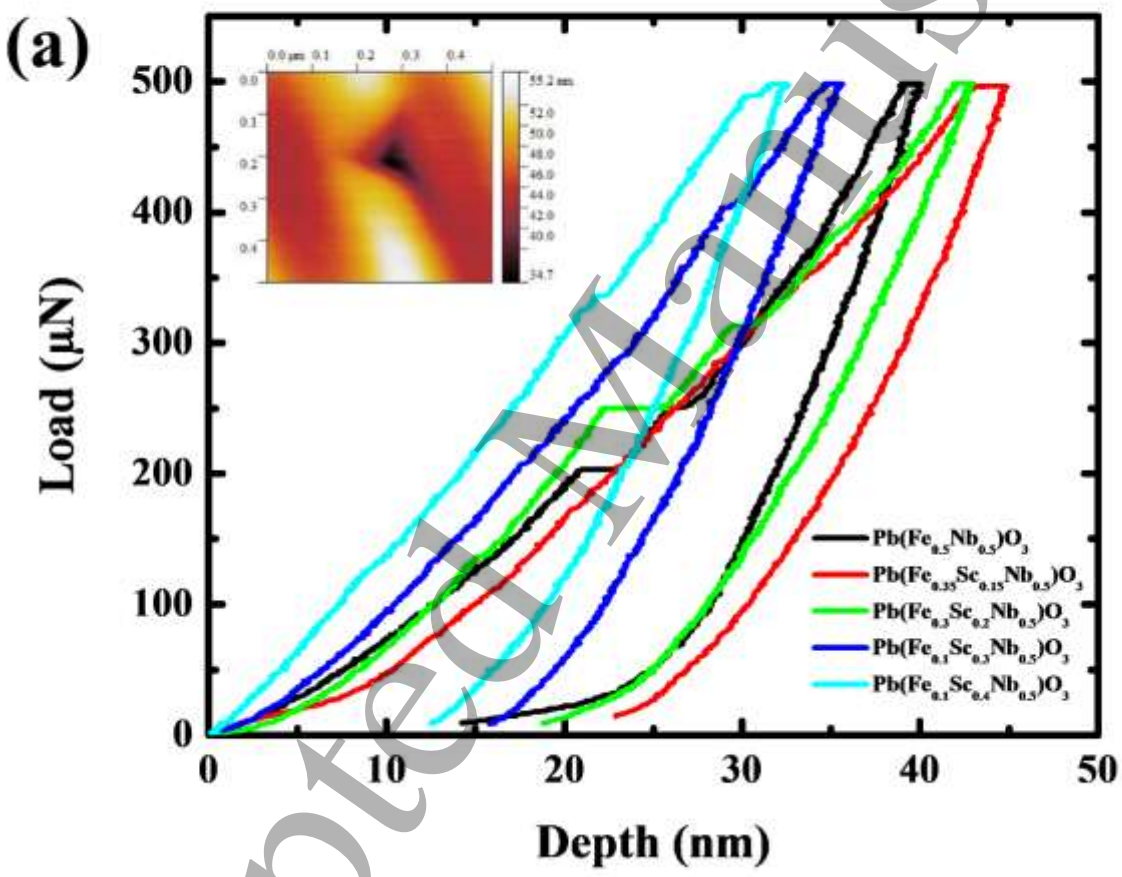

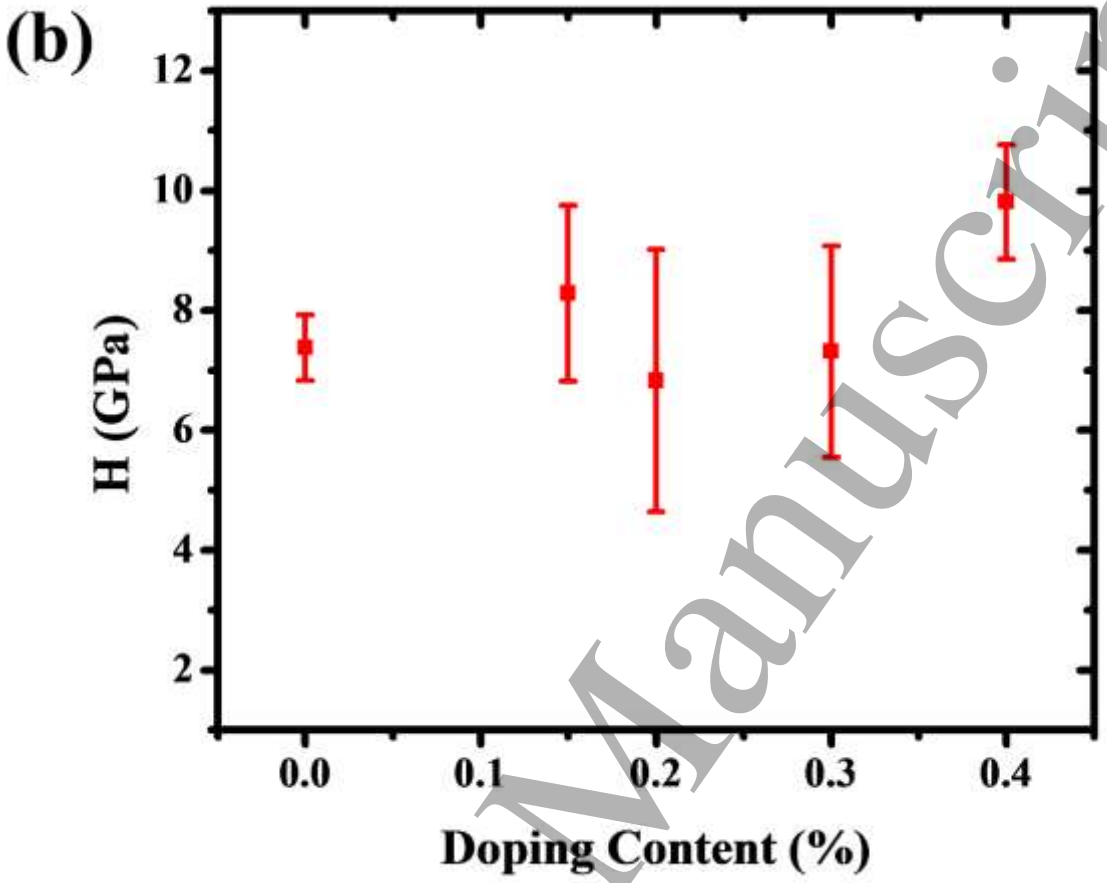

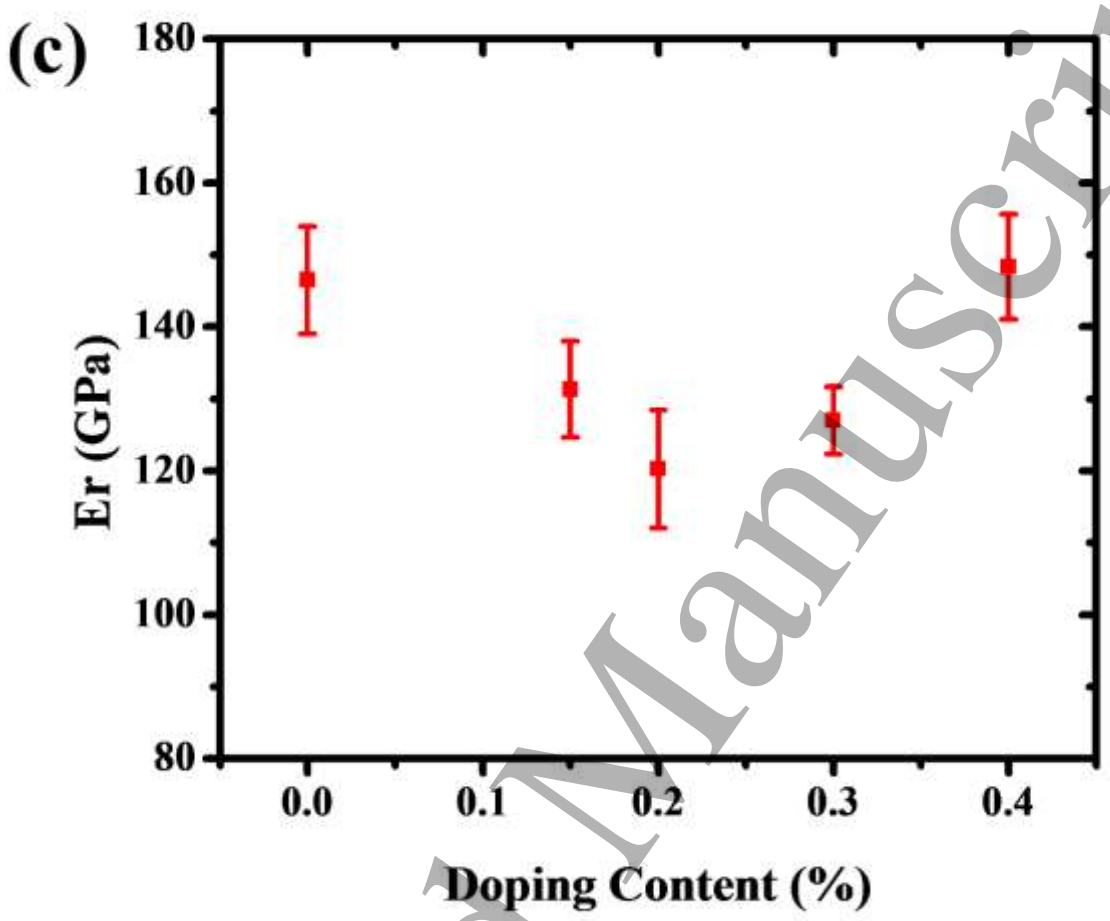

Figure 2a compares the loading unloading nanoindentation curves obtained from doped and undoped PFN samples at constant load of 500 μN. Inset shows a typical indent impression on to the surface of PFN00 sample. b) compares the average nanohardness and c) reduced modulus of pure PFN with doped samples.

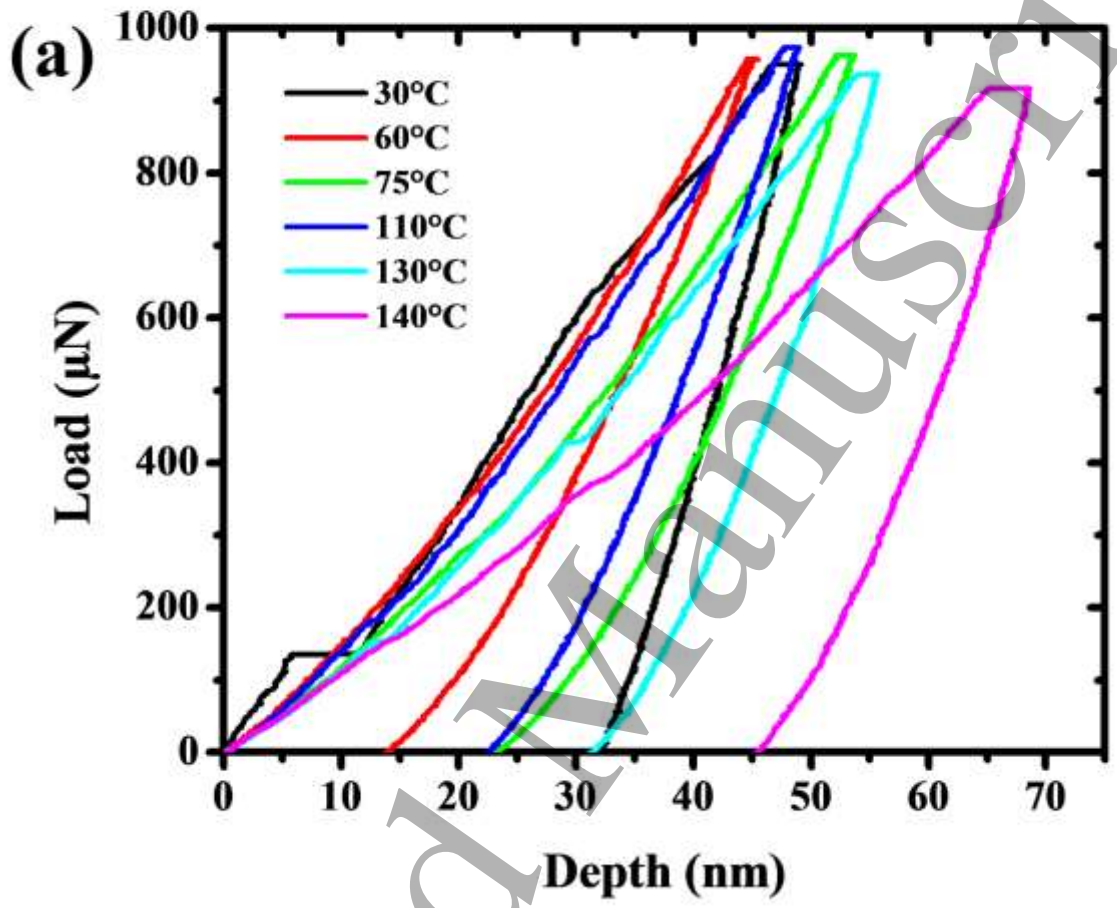

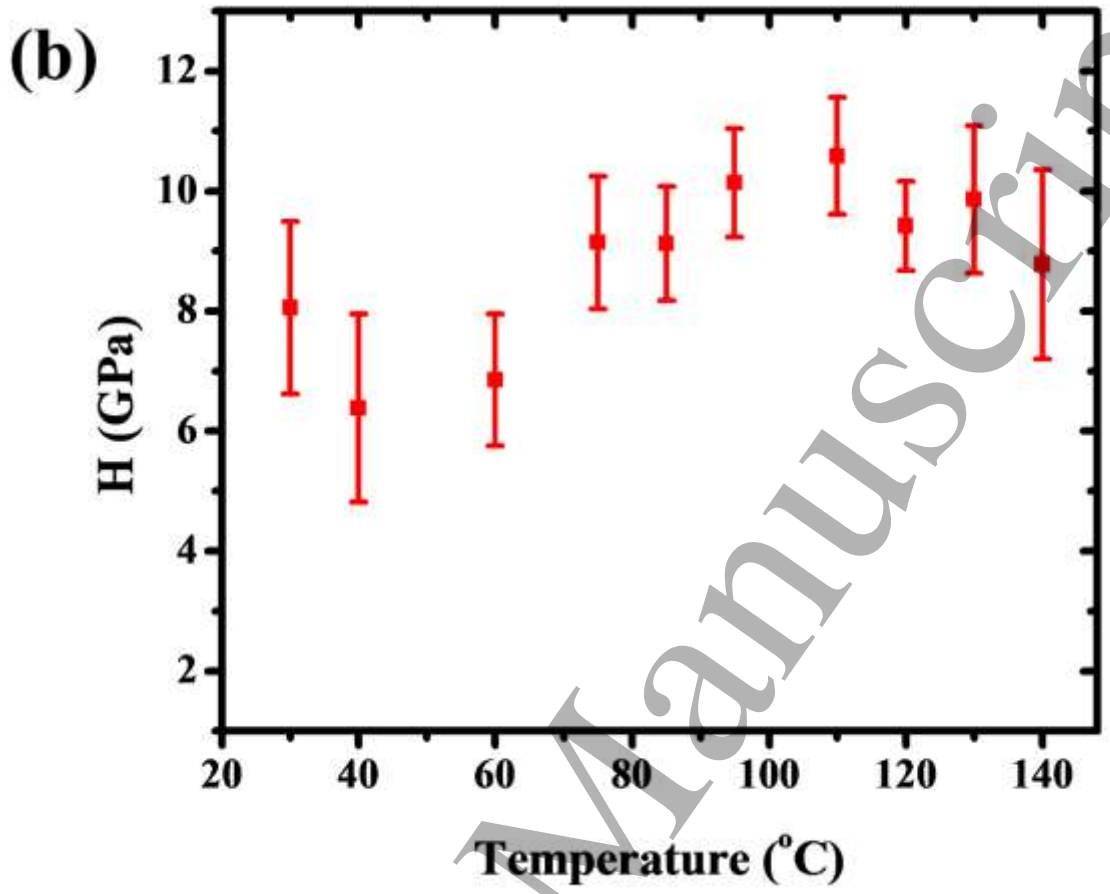

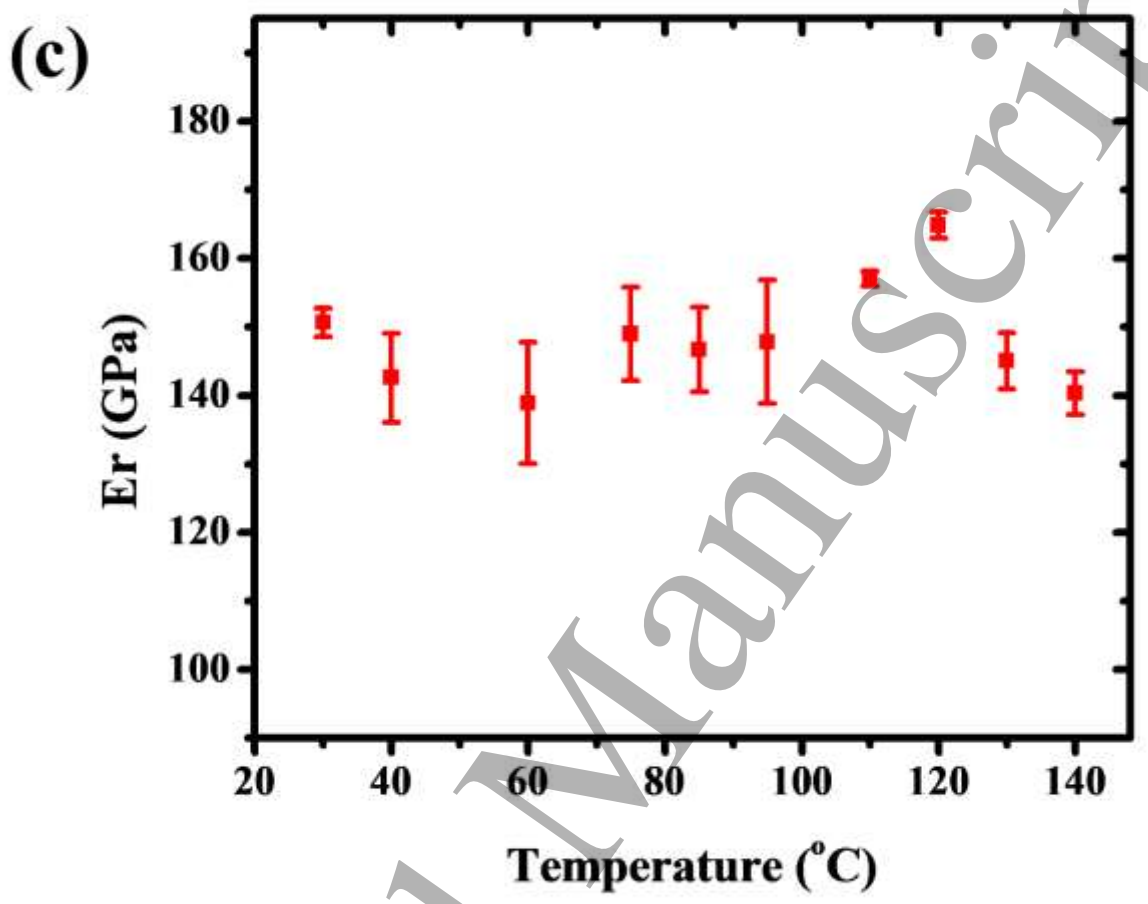

Figure 3a compares the loading-unloading nanoindentation curves obtained from PFN00 sample with increasing temperature from room temperature to 140 °C. b) average nanohardness and c) reduced modulus of pure PFN with increasing temperature.